This is a copy of the published version, or version of record, available on the publisher's website. This version does not track changes, errata, or withdrawals on the publisher's site.

Barocaloric properties of quaternary Mn3(Zn,In)N for room-temperature refrigeration applications

David Boldrin, Eduardo Mendive-Tapia, Jan Zemen, Julie B. Staunton, Angelo M. Gomes, Luis Ghivelder, John Halpin, Alexandra S. Gibbs, Araceli Aznar, Josep-Lluís Tamarit, Pol Lloveras, Xavier Moya, and Lesley F. Cohen

Published version information

Citation: D Boldrin et al. Barocaloric properties of quaternary Mn3(Zn,In)N for room-temperature refrigeration applications. Phys Rev B 104, no. 13 (2021): 134101

DOI: 10.1103/PhysRevB.104.134101

This version is made available in accordance with publisher policies. Please cite only the published version using the reference above. This is the citation assigned by the publisher at the time of issuing the APV. Please check the publisher's website for any updates.

This item was retrieved from **ePubs**, the Open Access archive of the Science and Technology Facilities Council, UK. Please contact epublications@stfc.ac.uk or go to http://epubs.stfc.ac.uk/ for further information and policies.

Barocaloric properties of quaternary $Mn_3(Zn,In)N$ for room-temperature refrigeration applications

David Boldrin,[1,2,*] Eduardo Mendive-Tapia,[3,4] Jan Zemen,[5] Julie B. Staunton,[4] Angelo M. Gomes,[6] Luis Ghivelder,[6] John Halpin,[2] Alexandra S. Gibbs,[7] Araceli Aznar,[8] Josep-Lluís Tamarit,[8] Pol Lloveras,[8] Xavier Moya,[9] and Lesley F. Cohen[1]

[1]*Department of Physics, Blackett Laboratory, Imperial College London, London SW7 2AZ, United Kingdom*
[2]*SUPA, School of Physics and Astronomy, University of Glasgow, Glasgow G12 8QQ, United Kingdom*
[3]*Department for Computational Materials Design, Max-Planck-Institut für Eisenforschung, 40237 Düsseldorf, Germany*
[4]*Department of Physics, University of Warwick, Coventry CV4 7AL, United Kingdom*
[5]*Faculty of Electrical Engineering, Czech Technical University in Prague, Technická 2, Prague 166 27, Czech Republic*
[6]*Instituto de Fisica, Universidade Federal do Rio de Janeiro, 21941-972 Rio de Janeiro, RJ, Brazil*
[7]*ISIS Facility, Rutherford Appleton Laboratory, Chilton, Didcot OX11 0QX, United Kingdom*
[8]*Departament de Física, EEBE, Campus Diagonal-Besòs and Barcelona Research Center in Multiscale Science and Engineering, Universitat Politècnica de Catalunya, Eduard Maristany, 10-14, 08019 Barcelona, Catalonia, Spain*
[9]*Department of Materials Science, University of Cambridge, Cambridge CB3 0FS, United Kingdom*

(Received 19 May 2021; accepted 1 September 2021; published 1 October 2021)

The magnetically frustrated manganese nitride antiperovskite family displays significant changes of entropy under hydrostatic pressure that can be useful for the emerging field of barocaloric cooling. Here we show that barocaloric properties of metallic antiperovskite Mn nitrides can be tailored for room-temperature application through quaternary alloying. We find an enhanced entropy change of $|\Delta S_t| = 37\ \mathrm{J\,K^{-1}\,kg^{-1}}$ at the $T_t = 300$ K antiferromagnetic transition of quaternary $Mn_3Zn_{0.5}In_{0.5}N$ relative to the ternary end members. The pressure-driven barocaloric entropy change of $Mn_3Zn_{0.5}In_{0.5}N$ reaches $|\Delta S_{BCE}| = 20\ \mathrm{J\,K^{-1}\,kg^{-1}}$ in 2.9 kbar. Our results open up a large phase space where compounds with improved barocaloric properties may be found.

DOI: 10.1103/PhysRevB.104.134101

I. INTRODUCTION

The field of caloric cooling offers opportunities for greater energy-efficient refrigeration without the need for environmentally harmful fluids. Magnetocalorics and electrocalorics are by far the most studied phenomena, with continued significant advances [1] although as yet without wide commercial uptake. Mechanocalorics including baro- and elastocalorics are only beginning to gain prominence [2,3], in part due to the perceived device engineering challenges combined with the relatively small range of materials displaying large mechanocaloric effects, particularly for barocalorics, the majority of which show large hysteresis. However, concerted efforts stimulated by significant increases in elastocaloric effects have recently led to design breakthroughs [4]. Driven by the ever-increasing magnitude of the barocaloric effects (BCE) reported [5,6], similar developments can be envisaged for a barocaloric device and have indeed recently been patented [7].

Manganese nitride antiperovskites (Mn_3AN) display a number of unusual properties, such as an anomalous coefficient of resistivity [8], negative thermal expansion [9], and piezomagnetism [10]. Recently, giant BCE have been reported in the A = Ga and Ni members of the family [10,11]. These effects originate from a noncollinear antiferromagnetic (AFM) order born from frustrated spin interactions, which strengthen with changes of volume and via feedback with the underlying electronic structure as magnetic order develops [10]. Both magnetovolume effects and the feedback with the electronic structure lead to a complex and rich mechanism that underpins the strongly first-order paramagnetic to AFM transition and hence the giant BCE properties [10]. As metals, their large density (important for compact applications) and high thermal conductivity (important for heat exchange) offer two important advantages for barocalorics over, e.g., ceramics and plastic crystals.

This work sets out to exploit the $Mn_3(A,B)N$ family's chemical flexibility, where the (A,B) site can be taken up by many transition and post-transition metals. We are motivated to investigate the effect of quaternary alloying on the barocaloric properties. The study is particularly pertinent given our recent observation of unexpectedly large barocaloric effects in Mn_3NiN, given the relatively small transitional volume change, originating from multisite magnetic exchange [10]. Moreover, quaternary alloying presents an ideal route to tailor the transition temperature, T_t, for refrigeration applications close to room temperature; A = Sn, Ge, In, and Pd all have T_t above 300 K, while the remainder (A = Zn, Co, Ag, Ni, Rh, Cu,...) lie below [9]. We study $Mn_3Zn_{1-x}In_xN$, where $T_t(\mathrm{Zn}, x = 1) = 180$ K and $T_t(\mathrm{In}, x = 0) = 380$ K, using dilatometry and temperature

*Corrsponding author: david.boldrin@glasgow.ac.uk

 ©2021 American Physical Society

and pressure dependent neutron diffraction, magnetometry, and calorimetry. We show that $Mn_3Zn_{0.5}In_{0.5}N$ undergoes a magnetic transition at $T_t = 300$ K with a concurrent volume change $|\frac{\Delta V_t}{V}| = 0.9\%$. This transition temperature decreases with pressure, $\frac{dT_t}{dp} = -3.3\ \mathrm{K\,kbar^{-1}}$, meaning the operational temperature is ideal for air conditioning. We find that $|\frac{\Delta V_t}{V}|$ is larger than expected in this material based on the sensitivity of T_t to pressure, $\frac{dT_t}{dp}$. Using the same framework we previously used to analyze Mn_3NiN, we show that multisite magnetic exchange terms appear responsible for the enhanced first-order nature of the transition in this material. The transitional entropy change of $|\Delta S_t| = 37\ \mathrm{J\,K^{-1}\,kg^{-1}}$ estimated from the Clausius-Clapeyron relation at zero pressure is larger than both the ternary end members and Mn_3GaN [11], while the pressure-driven barocaloric entropy change reaches 20 J $\mathrm{K^{-1}\,kg^{-1}}$ in 2.9 kbar. When normalizing by volume $|\Delta S_t| = 0.25\ \mathrm{J\,K^{-1}\,cm^{-3}}$, which is comparable to the colossal BCE close to room temperature recently found in plastic crystals, 0.42 and 0.48 $\mathrm{J\,K^{-1}\,cm^{-3}}$ for NPG and MNP (2-methyl-2-nitro-1-propanol), respectively [6], due to the ∼7 times larger density in the former. These results evidence the rich chemical phase space provided by $Mn_3(A, B)N$ that allows fine-tuning of the transition temperature and can lead to unexpected enhancement of their barocaloric properties.

II. EXPERIMENT

Samples were prepared using a standard solid state synthesis technique. First, $Mn_2N_{0.86}$ was prepared as detailed in Ref. [12]. Subsequently, the $Mn_2N_{0.86}$ precursor was ball milled and then thoroughly mixed by hand with elemental Zn (Sigma-Aldrich, 99.9% purity, 150 μm) and/or In powder (Sigma-Aldrich, 99.99% purity). The resulting mixture was pressed into ∼2 g pellets, wrapped in Ta foil, and sealed in evacuated quartz ampoules. The ampoules were heated to 780 °C for 2 days before being furnace cooled to room temperature. The regrinding, pelletization, and reaction steps were repeated if x-ray diffraction showed starting reagents to still be present.

Thermal expansion measurements were made with a silver based capacitance dilatometer [13] fitted in a PPMS system (manufactured by Quantum Design, Inc.). SEM-EDS and EBSD was performed using a Helios dual column plasma FIB-SEM.

Neutron diffraction was performed at the HRPD beamline at the ISIS neutron source, UK. Pressure dependent measurements were performed using a TiZr gas high-pressure cell. Data were also collected in a standard vanadium slab can on the same sample.

Pressure dependent calorimetry was performed using two different Cu-Be high-pressure cells that can operate in the temperature range 210–393 K, controlled by an external thermal bath. One is a MV1-30 cell (Unipress, Poland) adapted as a differential thermal analyzer by means of Peltier modules as thermal sensors, and that can operate in the pressure range 0–6 kbar. The other is a custom-built cell that uses Bridgman thermocouples as thermal sensors and that can operate in the pressure range 0–3 kbar. The sample was mixed with a perfluorinated fluid (Galden Bioblock Scientist) and encapsulated in a tin capsule. The pressure-transmitting fluid was DW-Therm M90.200.02 (Huber GmbH). Construction of the isobaric entropy-temperature curves is described in the Supplemental Material (SM) [14].

III. RESULTS AND DISCUSSION

We begin by characterizing the crystal and magnetic structures of $Mn_3Zn_{0.5}In_{0.5}N$ before turning to measurements of the barocaloric properties of $Mn_3Zn_{1-x}In_xN$ ($x = 0$, 0.5, and 1). We performed neutron diffraction measurements on the former as a function of temperature and applied pressure. Data were collected between 10 and 312 K at ambient pressure and between 0 and 5.4 kbar at 294 K on the HRPD beamline at ISIS, UK. Rietveld refinement of the data collected at 10 K is shown in Fig. 1(a) and was performed using the FULLPROF [16] and GSAS2 [17] software packages. Away from the transition region, the data are well fitted by a single antiperovskite phase with $Pm\bar{3}m$ symmetry and lattice parameter $a = 3.9475$ Å at 10 K. Due to the close neutron scattering lengths of Zn and In ($b_{Zn} = 5.68$ and $b_{In} = 4.065–0.0539i$ fm), combined with the significant absorption from In, the occupancies on this crystallographic site would not refine stably. However, the sharpness of the peaks demonstrates that the sample is highly crystalline with a well-defined stoichiometry. No improvement to the fit was observed when allowing the Mn or N site occupancy to refine. The magnetic Bragg peaks at 10 K are aligned with the nuclear peaks, meaning the magnetic propagation vector is $k = 0$. The magnetic peaks are refined well with the noncollinear AFM Γ^{5g} structure, using the notation of Fruchart *et al.* [18], with a moment size of $2.49\mu_B$ on each Mn site. Data collected on warming show no clear sign of a magnetic transition, evidenced by the temperature dependence of the (100) peak intensity in Fig. 1(b), until T_N where all magnetic Bragg peaks disappear. The same magnetic structure is found in Mn_3ZnN [19] (at high temperature), while it has also been proposed in Mn_3InN [20]. It is therefore clear that in this case alloying preserves the Γ^{5g} structure and does not induce competition with any additional magnetic phases.

Measurements performed as a function of temperature and pressure across the PM to AFM transition reveal the presence of regions where both phases exist. Figure 1(c) shows the temperature dependence of the (321) reflection intensity close to T_N and highlights the coexistence of two peaks which originate from the PM and AFM states of the sample (see Fig. S2 for the equivalent line plots [14]). This is clear evidence that the transition does not proceed uniformly throughout the sample and therefore a mixed phase region exists. We fitted both phases (PM and AFM) in the transition region using a le Bail technique to determine the volume change of each, shown in Fig. 1(d). The region in which both phases exist is 17 K between 290 and 307 K and the volume change of the individual phases within this region behaves almost linearly, as is expected. Interestingly, the lattice expansion of the AFM phase in the transition region is significantly larger than both the pretransitional region below 290 K and that of the PM phase within the transition region. Such behavior hints at anomalous contributions to the transition, such as an elastic instability.

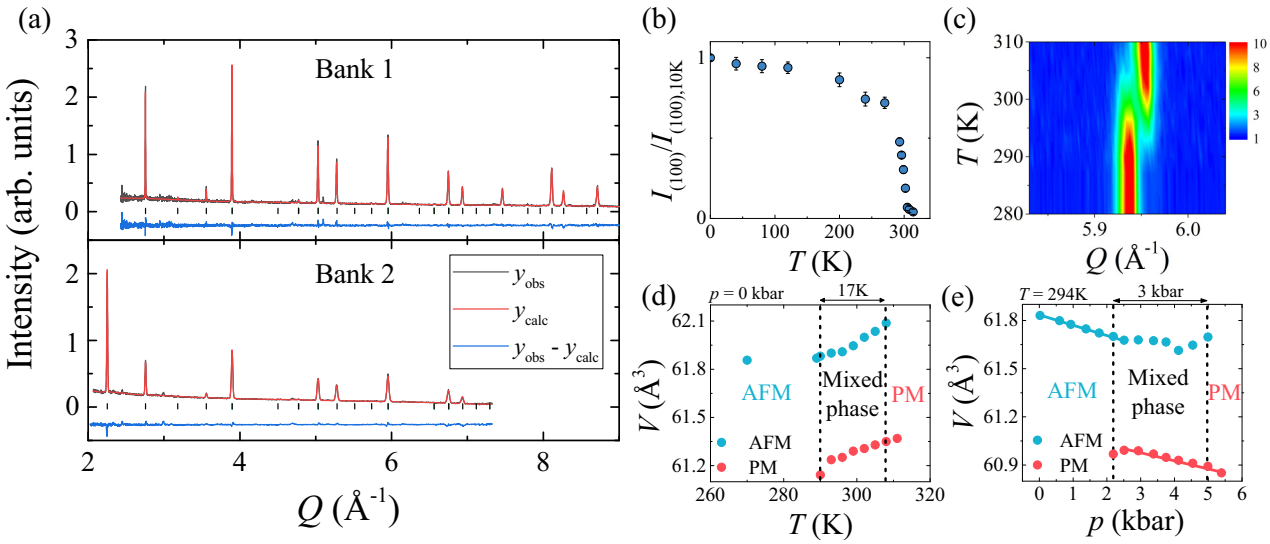

FIG. 1. (a) Rietveld refinement of powder neutron diffraction data collected at 10 K on banks 1 (backscattering) and 2 (90°) of HRPD, ISIS. Black tick marks indicate the reflections from the antiperovskite phase. The minor additional peaks, e.g., at $Q = 5.1$ Å^{-1}, are from MnO. (b) Temperature dependence of the fitted (100) peak intensity. (c) Thermodiffractogram of the (321) reflection. (d) Temperature dependence of the lattice volume at ambient pressure close to T_t for both the AFM and PM states. (e) Pressure dependence of the lattice volume at 294 K. Dotted vertical lines in (d) and (e) separate the single and mixed phase magnetic regimes, as described in the text. Solid lines in (e) are guides to the eye. Error bars in (d) and (e) are smaller than the symbol size.

The mixed phase region can also be mapped out when the transition is driven by pressure, with a width of 3 kbar, from the AFM to PM state. Figure 1(e) shows the isothermal volume change of both AFM and PM phases as a function of pressure at $T = 294$ K, again determined using a le Bail fitting. According to Fig. 1(d), at this temperature the sample should be in the mixed phase region; however, the diffraction data clearly shows that only the AFM phase is present (see Fig. S2c-d). This suggests a slight discrepancy between the temperature recorded in the standard sample holder and the pressure cell. Up until 2 kbar the volume of the AFM phase decreases linearly, as expected. Between 2 and 5 kbar, the PM phase appears and coexists with the AFM phase. The PM and AFM phases behave quite differently within the mixed phase region. The PM phase volume decreases linearly with increasing pressure. However, the AFM phase volume remains essentially constant between 2 and 4 kbar and increases sharply at pressures above this. Although we were unable to refine the magnetic structure from the data due to the large background from the pressure cell, the sharp change in volume of the AFM phase above 4 kbar strongly suggests that a magnetic transition occurs in this region and therefore that the Γ^{5g} structure is unstable to pressure. Nonetheless, the phase coexistence in both the pressure and temperature dependent measurements are evidence of the first-order behavior at the transition and suggest the presence of a barocaloric effect.

Moving to the barocaloric properties of the $x = 0$, 0.5, and 1 samples, we use the entropy change across the transition estimated using the Clausius-Clapeyron relation to compare between these and other antiperovskites. The relation is

$$\left|\Delta S_t^{CC}\right| = \Delta V_t \left(\frac{dT_t}{dp}\right)^{-1}, \quad (1)$$

where $|\Delta S_t^{CC}|$ is the entropy change from the Clausius-Clapeyron relationship, ΔV_t is the volume change at the transition, and $\frac{dT_t}{dp}$ is the rate of change of the transition temperature, T_t, with applied pressure, p. This provides a useful figure of merit (FOM) to allow comparison of BCE between similar materials (assuming the similar volumes of Mn_3AN and other metallic materials) given by FOM $= \frac{\Delta V_t}{V}(\frac{dT_t}{dp})^{-1}$ [11]. This FOM evaluates how large the discontinuity at the first-order PM-to-triangular AFM transition is, which directly relates to the size of the BCE.

As explained by Bean and Rodbell [21], the first-order character of a magnetic phase transition, and its magnitude, from the PM state to another ordered magnetic state can be attributed to the presence of an overall negative fourth-order coefficient in a Gibbs free energy, G (expanded in terms of a magnetic order parameter), caused by a magnetovolume coupling in magnetic materials. We have previously shown that magnetic exchange correlations between the local moments that are higher order than pairwise, i.e., multisite interactions, can also generate an overall negative fourth-order contribution in the free energy, thus driving and enhancing the first-order character of the magnetic phase transition in Mn_3AN [10]. As the electronic structure transforms due to different underlying states of magnetic order (e.g., paramagnetic, triangular antiferromagnetic, partially ordered, etc.), a feedback reaction is produced acting on the magnetic interactions between the local moments. This arises when different effective pairwise interactions would be obtained when calculated in different states of magnetic order. In order to capture this complexity, the interactions among the local moments, from the paramagnetic state at high T down to the low temperature magnetic ordered state, can instead be succinctly expressed in terms of pairwise plus higher order multisite interactions. This

TABLE I. Properties of various Mn_3AN materials relevant to their barocaloric effects. $\omega_{s,10\,K}$ is the spontaneous magnetostriction at 10 K between the PM and AFM states.

A	T_N (K)	$\lvert\frac{\Delta V_t}{V}\rvert$ (%)	$\frac{dT_t}{dp}$ (K kbar^{-1})	$\lvert\frac{\Delta V_t}{V}\rvert(\frac{dT_t}{dp})^{-1}$ (% kbar K^{-1} $\times 10^{-1}$)	$\omega_{s,10\,K}$ (%)	$\lvert\Delta S_t^{CC}\rvert$ (J K^{-1} kg^{-1})	$\lvert\Delta S_t\rvert$ (J K^{-1} kg^{-1})	c_{mv} (meV)	$\mathcal{S}^{(4)}$ (meV)
Ni [10]	262	0.4	−1.3	3.1	0.8	47	47	250	13
Ga [9,11]	288	1.0	−6.5	1.5	2.0	22	22	1107	−25
Zn	186	1.5 [9][a]	−7.0	2.1	2.0 [9]	32	39 [26]	1267	−40
$Zn_{0.5}In_{0.5}$	300	0.9	−3.3	2.9	1.8[b]	37	37	600	6
In	380	0.3 [9][a]	−3.5	0.9	0.9 [9]	12		650	6

[a]The volume change is given by $\lvert\frac{\Delta V_t}{V}\rvert = 3\frac{dL}{L}$, where $\frac{dL}{L}$ is taken from [9].
[b]Obtained through the neutron diffraction data.

framework describes the feedback between the electronic structure and the configuration of the local magnetic moments. This effect can arise in situations where the crystal structure remains unperturbed, i.e., where the interaction is purely electronic in nature, or as in this case where there are both electronic and lattice interactions to consider [22].

We determine the effect of both magnetovolume coupling and of multisite interactions by studying G containing a hierarchy of local moment correlations, i.e., second- and higher-order free energy magnetic terms [22]. The form of G here emerges from previous first-principles studies of frustrated AFM materials and other magnetic systems at finite temperature [10,22–24]. However, in this work we extract the coefficients of G instead from our experimental data as described in Ref. [10]. Our theoretical approach allows us to distinguish magnetovolume and purely electronic mechanisms, and their effect on the magnetic phase transition:

$$\begin{aligned} G = &-\mathcal{S}^{(2)}\left(M_1^2+M_2^2+M_3^2\right) - \mathcal{S}^{(4)}\left(M_1^4+M_2^4+M_3^4\right) \\ &- c_{mv}\frac{\Delta V_t}{V}\left(M_1^2+M_2^2+M_3^2\right) \\ &+ \frac{1}{2}\gamma\frac{\Delta V_t^2}{V} + \Delta V_t p - T S_{tot}, \end{aligned} \tag{2}$$

where $\mathcal{S}^{(2)}$ contains the effect of pairwise interactions, $\mathcal{S}^{(4)}$ arises from quartic multisite contributions, M_i is the magnetic order parameter, c_{mv} is the lowest order possible magnetovolume coupling, ΔV_t is the volume change at the transition, V is the volume of the unit cell in the paramagnetic state, γ is the bulk modulus, and S_{tot} is the total entropy coming from orientational magnetic degrees of freedom [22]. We highlight that the number of free energy coefficients has been reduced to the lowest possible by exploiting symmetry arguments of this crystal structure. The magnitudes of $\mathcal{S}^{(2)}$, $\mathcal{S}^{(4)}$, and c_{mv} are obtained by performing a fitting of the experimental values of T_N, $\frac{dT_t}{dp}$, and ΔS (or the spontaneous volume change) to the corresponding predicted values of these quantities obtained after minimizing Eq. (2) with respect to M_i [10]. Albeit the fitting of these three parameters is done simultaneously, we highlight that the magnitudes of $\mathcal{S}^{(2)}$ and c_{mv} are mainly given by T_N and $\frac{dT_t}{dp}$, respectively, while $\mathcal{S}^{(4)}$ depends on the overall effect of the total fourth-order contribution in G, including that from c_{mv}, giving rise to the first-order character and the size of the BCE. The value of the bulk modulus, $\gamma \sim 130$ GPa, is taken directly from experiment [9] and S_{tot} follows an analytical expression in terms of M_i only, which is derived from a mean-field theory [22,25]. Minimizing Eq. (2) with respect to $\frac{\Delta V_t}{V}$ gives $\frac{\Delta V_t}{V} = \frac{c_{mv}}{V\gamma}(M_1^2+M_2^2+M_3^2) - \frac{p}{\gamma}$, which substituted into Eq. (2) shows how the magnetovolume coupling generates a fourth-order free term on M_i [10]. It is therefore apparent that either the magnetovolume coupling, c_{mv}, or multisite interactions, $\mathcal{S}^{(4)}$, can drive the first-order transition [10] since they generate fourth-order free energy coupling [21]. We previously found that the multisite interactions enhance first-order character in Mn_3NiN, relative to Mn_3GaN, despite a smaller $\frac{dT_t}{dp}$ and magnetovolume coupling [10]. The values of these interactions, $\mathcal{S}^{(4)}$, are given in Table I , where being positive (negative) generates a negative (positive) total contribution in G and therefore acts to stabilize (destabilize) the triangular AFM structure. We find for Mn_3ZnN the first-order behavior is largely driven by magnetovolume coupling as c_{mv} is large and $\mathcal{S}^{(4)}$ is negative. For Mn_3InN, the magnetovolume coupling is significant and $\mathcal{S}^{(4)}$ is positive; however, the small volume change means the entropy change, $\lvert\Delta S_t^{CC}\rvert$, is also small.

We now turn to the pertinent results recorded in Table I on the $x = 0.5$ sample of the series $Mn_3Zn_{1-x}In_xN$. Figure 2(a) shows the volume as a function of temperature measured using dilatometry, which demonstrates a large volume increase of $\lvert\frac{\Delta V_t}{V}\rvert = 0.9\%$ at the PM-AFM transition, $T_N \sim 300$ K. This volume change also leads to a large spontaneous magnetostriction, $\omega_{s,10\,K}$ (see Table I), a property that has previously been used to characterize Mn_3AN [9]. The value reported here is of similar magnitude to the largest values found in $A =$ Zn and Ga. The heat flow data shown in Fig. 2(b) gives an entropy change at the transition of $\Delta S_t = 37.4 \pm 0.2$ and -37.6 ± 0.2 J K^{-1} kg^{-1} on warming and cooling, respectively. The linear dependence of T_N with pressure measured using pressure dependent calorimetry gives $\frac{dT_t}{dp} = -3.3 \pm 0.2$ K kbar^{-1}. This allows us to estimate the entropy change at the transition using the Clausius-Clapeyron relation, which gives a value of $\lvert\Delta S_t^{CC}\rvert = 37 \pm 2$ J K^{-1} kg^{-1} in excellent agreement with the measured $\lvert\Delta S_t\rvert$. Using the same method described for the ternary end members, we also extracted c_{mv} and $\mathcal{S}^{(4)}$ for the $x = 0.5$ compound by minimizing Eq. (2) as explained above.

We can now make some comparisons between the ternary end members and the quaternary sample. It is clear that the magnitude of the transitional volume change of the quaternary sample lies roughly in between the two end members, suggesting a linear relationship of $\lvert\frac{\Delta V_t}{V}\rvert$ on alloying. The behavior

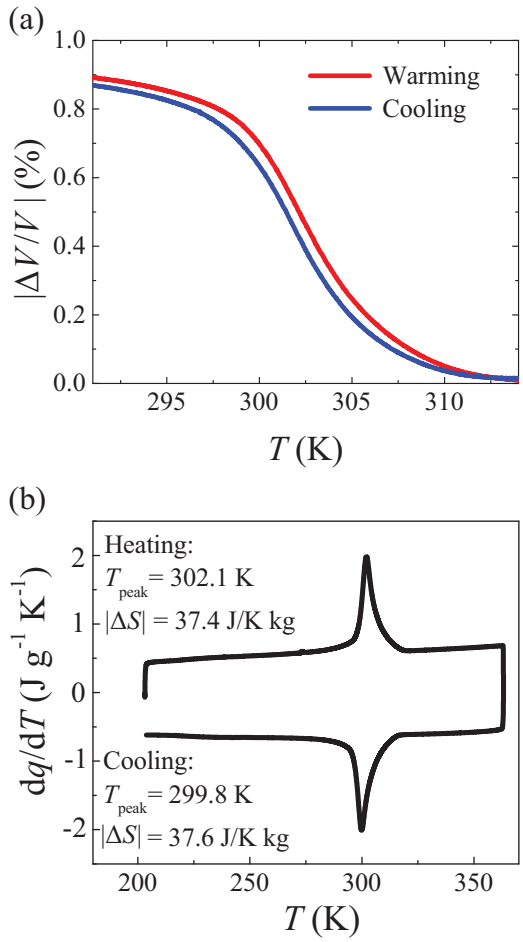

FIG. 2. (a) Volume change of $Mn_3Zn_{0.5}In_{0.5}N$ as a function of temperature measured using dilatometry, where $\frac{\Delta V}{V}$ is calculated from the measured $\frac{dL}{L}$ using $\frac{\Delta V}{V} = 3^* \frac{dL}{L}$. (b) Temperature dependent heat flow measurements at normal pressure.

of $\frac{dT_t}{dp}$ is quite different as it is roughly the same for the $x = 0.5$ and 1 samples, whereas it is significantly larger for the $x = 0$. Given the behavior of these two parameters, the resulting $|\Delta S_t^{CC}|$ after applying Eq. (1) is significantly larger for the $x = 0.5$ sample compared to the end members. These results clearly demonstrate that unexpected enhancements in the first-order nature of the transition can be achieved through quaternary alloying.

As expected from the $\frac{dT_t}{dp}$ values, the magnetovolume coupling, c_{mv}, is similar for the $x = 0.5$ and 1 samples, whereas it is significantly larger for the $x = 0$. Interestingly, a similar behavior is found for $\mathcal{S}^{(4)}$; the value is positive for $x = 0.5$ and 1, whereas it is large and negative for $x = 0$. The overall effect of the multisite Mn spin interactions, described by $\mathcal{S}^{(4)}$, is to stabilize (or destabilize) the noncollinear AFM structure for defined positive (or negative) values of $\mathcal{S}^{(4)}$. We previously found that these interactions enhance first-order character in Mn_3NiN and produce a large transitional volume change relative to the magnetovolume coupling [10], evidenced by the large FOM, $\frac{\Delta V_t}{V}(\frac{dT_t}{dp})^{-1}$, in Table I. For $Mn_3Zn_{0.5}In_{0.5}N$ this ratio is similar to Mn_3NiN and indeed both have positive $\mathcal{S}^{(4)}$ terms, suggesting the multisite magnetic exchange plays an important role in enhancing the first-order transition in both. For Mn_3ZnN this ratio is of similar magnitude to Mn_3GaN and both have negative $\mathcal{S}^{(4)}$, which implies that magnetovolume coupling drives the first-order transition. For Mn_3InN this ratio is significantly smaller than all other samples yet its $\mathcal{S}^{(4)}$ term is positive. This may stem from the larger transition temperature, $T_t = 380$ K, meaning that the effect of $\mathcal{S}^{(4)}$ is comparatively smaller compared to $Mn_3Zn_{0.5}In_{0.5}N$. Further work on Mn_3InN is required to make an accurate comparison, for instance, by determining whether the same noncollinear AFM structure is present.

We now focus on the pressure driven barocaloric effects of $Mn_3Zn_{0.5}In_{0.5}N$. In Figs. 3(a) and 3(b), we show heat flow data measured as a function of temperature at different pressures. Integration of the heat flow data at different pressures allows us to construct isobaric entropy curves as shown in Figs. 3(c) and 3(d) (see SM for a full description). The latter is used to determine the barocaloric entropy change, $|\Delta S_{BCE}|$ [Figs. 3(e) and 3(f)], and adiabatic temperature change, ΔT_{AD} [Figs. 3(g) and 3(h)], for a given pressure across the transition, using quasidirect methods as previously described elsewhere [10]. We find that the magnitudes of $|\Delta S_{BCE}|$ and ΔT_{AD} are significantly larger when measured on cooling than on warming; however, the cause of this is unclear. At the highest applied pressure (4.2 kbar) the maximum on cooling of $\Delta S_{BCE} = -22 \pm 3\,\mathrm{J\,kg^{-1}\,K^{-1}}$ and $\Delta T_{AD} = 8.5 \pm 1$ K. While in principle $|\Delta S_{BCE}|$ should be similar to $|\Delta S_t|$, the former is less than $|\Delta S_t|$ (indicated in Table I) due to broadening of the transition, with the sharp first-order-like change giving a reduced entropy change $|\Delta S_{t,1}| = 26.3\,\mathrm{J\,kg^{-1}\,K^{-1}}$ (see Fig. S1 [14]). This latter number is in good agreement with $|\Delta S_{BCE}|$ from our quasidirect BCE measurements [see Fig. 3(e)], and it is expected that the two values would be in closer agreement at higher pressures as $|\Delta S_{BCE}|$ is not saturated at 4.2 kbar. Consistently, the phase coexistence region between $290 < T\,(\mathrm{K}) < 308$ in the neutron diffraction data roughly aligns with the sharp region in the heat flow data, corresponding to the first-order transition. To attempt to better understand the origin of this pretransitional region, we performed SEM-EDX compositional analysis combined with EBSD. The data show a partial segregation of In to grain boundaries (see Fig. S3 [14]) leaving the grain centers Zn rich (see Table S1). The sharpness of the neutron diffraction peaks demonstrates that the sample does not consist of a range of stoichiometries with varying Zn/In ratios, and therefore it appears this segregation is limited to a small volume percent of the sample at the grain boundary region. Nonetheless it may explain the increased pretransitional region of the transition. Further reaction steps, in an attempt to homogenize the sample, did not lead to stronger first-order behavior.

We now discuss the observed properties of $Mn_3Zn_{0.5}In_{0.5}N$ in the context of other studies of quaternary alloying in this antiperovskite family. Anomalous behavior in $Mn_3(A, B)N$ materials obtained by quaternary alloying has previously been demonstrated and related to the geometrically frustrated nature of the nearest-neighbor AFM interactions. For instance, it was previously observed that in the $Mn_3(Cu_{1-x}, Ge_x)N$ and $Mn_3(Cu_{1-y}, Sn_y)N$ series increased x or y doping (i) induces

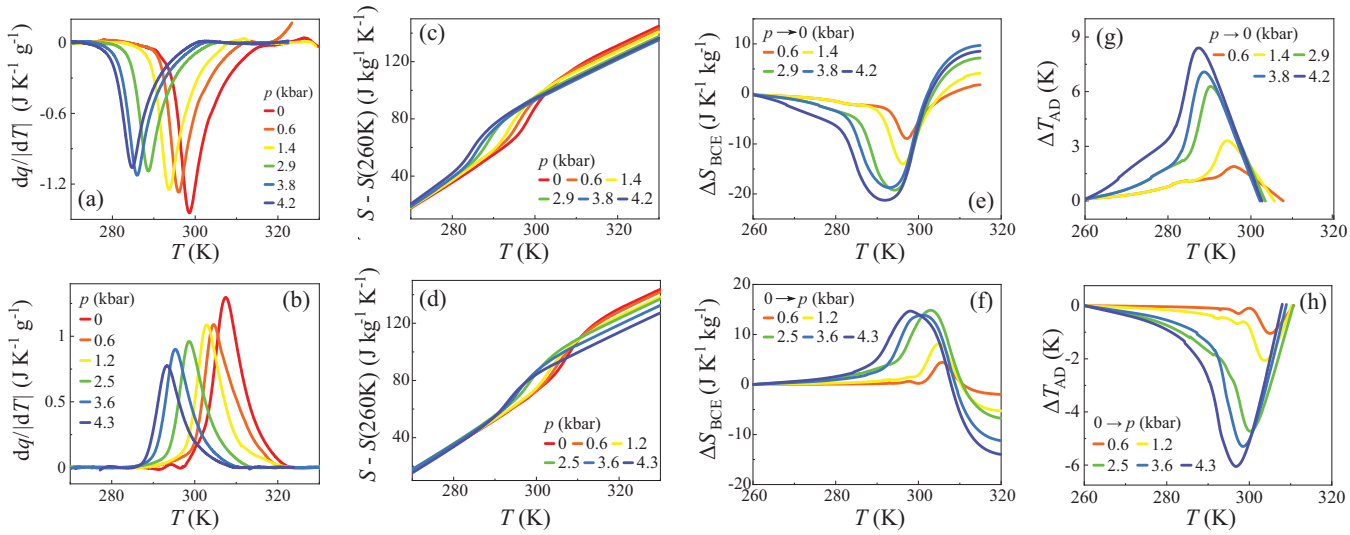

FIG. 3. Temperature dependent heat flow measurements measured on (a) cooling and (b) warming at various pressures. Isobaric entropy curves at different applied pressures on (c) cooling and (d) warming, extracted from the data in (a) and (b), respectively. Isothermal entropy change under (e) removal or (f) application of different pressures (BCE). Adiabatic temperature change under (g) removal or (h) application of different pressures.

unexpectedly large $|\frac{\Delta V_t}{V}|$ compared to the end members and (ii) reduces the volume of the PM state [9]. This was proposed to arise from strong magnetovolume coupling of the frustrated AFM interactions, which assists lattice contraction and reduces the PM lattice volume as well as suppressing the spin fluctuations in the PM phase. In particular, in the case of Mn_3GaN Matsunami *et al*. concluded that the giant BCE is attributable to such a magnetically frustrated mechanism principally owing to the strong magnetovolume coupling enhancing the change of volume with pressure [11], in agreement with our findings.

Our results show that magnetic frustration generates a more complex origin for the giant BCEs in antiperovskite materials. As we previously found for Mn_3NiN, the higher order multisite exchange effects, captured by $\mathcal{S}^{(4)}$, add to the effect of magnetovolume coupling to enhance the first-order character in $Mn_3Zn_{0.5}In_{0.5}N$. Both of these stem directly from the geometrically frustrated magnetism. In addition, the presence of $\mathcal{S}^{(4)}$ and its stabilizing effect on the AFM structure allows $\frac{dT_t}{dp}$ to remain small relative to the large discontinuity at the magnetic phase transition, with an associated larger BCE. Taken together, alloying has produced an entropy change larger than anticipated based on the values of the ternary end members. Our results clearly demonstrate that alloying can allow both control of T_t and enhancement of the BCE relative to the end members, exploiting two different aspects of the transition.

IV. CONCLUSIONS

We have tailored large barocaloric effects at room temperature by alloying members of the $Mn_3(A, B)N$ antiperovskite series with (i) large transitional volume changes and (ii) transitions positioned either side of room temperature. We find a large entropy change at the first-order transition at 300 K in the material $Mn_3Zn_{0.5}In_{0.5}N$ and show that this is due to a large volume change relative to the sensitivity of the transition to pressure. Similar to Mn_3NiN, a larger volume change occurs than expected when considering magnetovolume coupling alone, which is explained by the presence of multisite magnetic exchange. The latter enhances the first-order behavior and the barocaloric response relative to other materials with similar or larger spontaneous transitional volume changes, e.g., Mn_3GaN. Such a multisite magnetic term in the free energy captures how the intrinsic geometrically frustrated AFM interactions strengthen with magnetic ordering, strongly stabilizing the Γ^{5g} AFM structure. Pressure dependent neutron diffraction measurements reveal a mixed AFM-PM phase that exists close to the transition, when driven by temperature or pressure, which evidences the first-order nature of the transition. Our results further demonstrate the potential of quaternary alloying, opening up a vast phase space to explore $Mn_3(A, B)N$ for barocalorics and many other areas where these materials are being considered important for applications, such as spintronics [27,28], strain-driven caloric cooling in thin films [23], and energy conversion [29].

ACKNOWLEDGMENTS

We thank A. S. Wills for help with sample preparation. This work was supported by EPSRC (UK) Grants (No. EP/P511109/1, No. EP/P030548/1, No. EP/J06750/1, and No. EP/M028941/1), MINECO Project No. FIS2017-82625-P, and ERC Starting Grant No. 680032. D.B. is grateful for support from a Leverhulme Trust Early Career Fellowship (No. ECF-2019-351) and a University of Glasgow Lord Kelvin Adam Smith Fellowship. X.M. is grateful for support from the Royal Society. A.M.G. and L.G. acknowledge financial support from the Brazilian Agencies FAPERJ and CNPq. Experiments at the ISIS Neutron and Muon Source were supported by a beamtime allocation from the Science and Technology Facilities Council, see Ref. [30].

[1] B. Nair, T. Usui, S. Crossley, S. Kurdi, G. G. Guzmán-Verri, X. Moya, S. Hirose, and N. D. Mathur, Large electrocaloric effects in oxide multilayer capacitors over a wide temperature range, Nature (London) **575**, 468 (2019).

[2] L. Mañosa and A. Planes, Materials with giant mechanocaloric effects: Cooling by strength, Adv. Mater. **29**, 1603607 (2017).

[3] X. Moya, S. Kar-Narayan, and N. D. Mathur, Caloric materials near ferroic phase transitions, Nat. Mater. **13**, 439 (2014).

[4] J. Tušek, K. Engelbrecht, D. Eriksen, S. Dall'Olio, J. Tušek, and N. Pryds, A regenerative elastocaloric heat pump, Nat. Energy **1**, 16134 (2016).

[5] P. Lloveras, A. Aznar, M. Barrio, P. Negrier, C. Popescu, A. Planes, L. Mañosa, E. Stern-Taulats, A. Avramenko, N. D. Mathur, X. Moya, and J.-L. Tamarit, Colossal barocaloric effects near room temperature in plastic crystals of neopentylglycol, Nat. Commun. **10**, 1803 (2019).

[6] B. Li, Y. Kawakita, S. Ohira-Kawamura, T. Sugahara, H. Wang, J. Wang, Y. Chen, S. I. Kawaguchi, S. Kawaguchi, K. Ohara, K. Li, D. Yu, R. Mole, T. Hattori, T. Kikuchi, S.-i. Yano, Z. Zhang, Z. Zhang, W. Ren, S. Lin *et al.*, Colossal barocaloric effects in plastic crystals, Nature (London) **567**, 506 (2019).

[7] X. Moya, A. Avramenko, L. Mañosa, J.-L. Tamarit, and P. Lloveras, Use of barocaloric materials and barocaloric devices, PCT/EP2017/076203 (2017).

[8] E. O. Chi, W. S. Kim, and N. H. Hur, Nearly zero temperature coefficient of resistivity in antiperovskite compound $CuNMn_3$, Solid State Commun. **120**, 307 (2001).

[9] K. Takenaka, M. Ichigo, T. Hamada, A. Ozawa, T. Shibayama, T. Inagaki, and K. Asano, Magnetovolume effects in manganese nitrides with antiperovskite structure, Sci. Technol. Adv. Mater. **15**, 15009 (2014).

[10] D. Boldrin, E. Mendive-Tapia, J. Zemen, J. B. Staunton, T. Hansen, A. Aznar, J.-L. Tamarit, M. Barrio, P. Lloveras, J. Kim, X. Moya, and L. F. Cohen, Multisite Exchange-Enhanced Barocaloric Response in Mn_3NiN, Phys. Rev. X **8**, 041035 (2018).

[11] D. Matsunami, A. Fujita, K. Takenaka, and M. Kano, Giant barocaloric effect enhanced by the frustration of the antiferromagnetic phase in Mn_3GaN, Nat. Mater. **14**, 73 (2014).

[12] D. Boldrin and L. F. Cohen, The role of competing magnetic interactions on the abnormal expansion properties in manganese antiperovskites, $Mn_{3+x}A_{1-x}N$ (A = Ni, Sn), J. Alloys Compd. **699**, 887 (2017).

[13] M. Rotter, H. Müller, E. Gratz, M. Doerr, and M. Loewenhaupt, A miniature capacitance dilatometer for magnetostriction and thermal expansion measurements, Rev. Sci. Instrum. **69**, 2742 (1998).

[14] See Supplemental Material at http://link.aps.org/supplemental/10.1103/PhysRevB.104.134101 for a description of the isobaric entropy-temperature curve construction, chemical compositional analysis, and neutron diffraction data. Reference [15] is contained within.

[15] E. Stern-Taulats, A. Gràcia-Condal, A. Planes, P. Lloveras, M. Barrio, J. L. Tamarit, S. Pramanick, S. Majumdar, and L. Mañosa, Reversible adiabatic temperature changes at the magnetocaloric and barocaloric effects in $Fe_{49}Rh_{51}$, Appl. Phys. Lett. **107**, 152409 (2015).

[16] J. Rodriguez-Carvajal, Recent advances in magnetic structure determination by neutron powder diffraction, Phys. B: Condens. Matter **192**, 55 (1993).

[17] B. H. Toby and R. B. Von Dreele, GSAS-II: The genesis of a modern open-source all purpose crystallography software package, J. Appl. Crystallogr. **46**, 544 (2013).

[18] D. Fruchart and E. F. Bertaut, Magnetic studies of the metallic perovskite-type compounds of manganese, J. Phys. Soc. Jpn. **44**, 781 (1978).

[19] D. Fruchart, E. F. Bertaut, R. Madar, and R. Fruchart, Diffraction neutronique de Mn_3ZnN, J. Phys. Colloq. **32**, C1-876 (1971).

[20] *Landolt-Bornstein, New Series III/19c* (Springer-Verlag, Berlin, 1981).

[21] C. Bean and D. Rodbell, Magnetic Disorder at a First Order Phase Transformation, Phys. Rev. **126**, 104 (1962).

[22] E. Mendive-Tapia and J. B. Staunton, Ab initio theory of the Gibbs free energy and a hierarchy of local moment correlation functions in itinerant electron systems: The magnetism of the Mn_3A materials class, Phys. Rev. B **99**, 144424 (2019).

[23] J. Zemen, E. Mendive-Tapia, Z. Gercsi, R. Banerjee, J. B. Staunton, and K. G. Sandeman, Frustrated magnetism and caloric effects in Mn-based antiperovskite nitrides: *Ab initio* theory, Phys. Rev. B **95**, 184438 (2017).

[24] E. Mendive-Tapia and J. B. Staunton, Theory of Magnetic Ordering in the Heavy Rare Earths: Ab Initio Electronic Origin of Pair- and Four-Spin Interactions, Phys. Rev. Lett. **118**, 197202 (2017).

[25] B. L. Gyorffy, A. J. Pindor, J. Staunton, G. M. Stocks, and H. Winter, A first-principles theory of ferromagnetic phase transitions in metals, J. Phys. F **15**, 1337 (1985).

[26] J. García, R. Navarro, J. Bartolomé, R. Burriel, D. González, and D. Fruchart, Specific heat of the cubic metallic perovskites Mn_3ZnN and Mn_3GaN, J. Magn. Magn. Mater. **15–18**, 1155 (1980).

[27] J. Zemen, Z. Gercsi, and K. G. Sandeman, Piezomagnetic effect as a counterpart of negative thermal expansion in magnetically frustrated Mn-based antiperovskite nitrides, Phys. Rev. B **96**, 024451 (2017).

[28] D. Boldrin, I. Samathrakis, J. Zemen, A. Mihai, B. Zou, F. Johnson, B. D. Esser, D. W. McComb, P. K. Petrov, H. Zhang, and L. F. Cohen, Anomalous Hall effect in noncollinear antiferromagnetic Mn_3NiN thin films, Phys. Rev. Materials **3**, 094409 (2019).

[29] X. Zhou, J.-P. Hanke, W. Feng, S. Blügel, Y. Mokrousov, and Y. Yao, Giant anomalous Nernst effect in noncollinear antiferromagnetic Mn-based antiperovskite nitrides, Phys. Rev. Materials **4**, 024408 (2020).

[30] Doi: 10.5286/ISIS.E.RB1810625.